Synthesis of hybrid silver–doped graphene oxide material as a superior antibacterial performance and cadmium ion sensor

Nguyen Thi Thuy Linh[1,2,3], Che Quang Cong[1,2,3], Nguyen Minh Dat[1,3], Tran Chau Diep[1,3], Ninh Thi Tinh[1,3], Doan Ba Thinh[2,3], Nguyen Thanh Hoai Nam[2], Chau Gia Khang[2], Le Thi Bich Lieu[1,2,3], Doan Thi Yen Oanh[4], Hoang Minh Nam[1,2,3], Mai Thanh Phong[1,2,3], Nguyen Huu Hieu[1,2,3*]

[1]VNU–HCM Key Laboratory of Chemical Engineering and Petroleum Processing (Key CEPP Lab), Ho Chi Minh City University of Technology, 268 Ly Thuong Kiet Street, District 10, Ho Chi Minh City 70000, Vietnam
[2]Faculty of Chemical Engineering, Ho Chi Minh City University of Technology, 268 Ly Thuong Kiet Street, District 10, Ho Chi Minh City 70000, Vietnam
[3]Vietnam National University Ho Chi Minh City, Linh Trung Ward, Thu Duc District, Ho Chi Minh City 70000, Vietnam
[4]Publishing House for Science Technology, Vietnam Academy of Science and Technology, 18 Hoang Quoc Viet, Cau Giay, Hanoi 10000, Vietnam
*Email: nhhieubk@hcmut.edu.vn

ARTICLE INFO

ABSTRACT

In this study, *in-situ* method was applied for synthesizing silver-doped graphene oxide (Ag/GO). The material was extensively characterized by X-ray diffraction, Transmission electron microscopy, Scanning electron microscope, Raman spectroscopy, energy-dispersive X-ray spectroscopy, and UV-Vis spectroscopy. The characterization analysis results demonstrated that Ag/GO nanocomposite was successfully synthesized, revealing the formation of AgNPs on GO sheets with an average diameter ranging from 15 to 30 nm. The Ag/GO nanocomposite exhibited excellent antibacterial effect against three strains of Gram-negative (*Escherichia coli*, *Pseudomonas aeruginosa*), and Gram-positive (*Staphylococcus aureus*) bacteria using the zone inhibition method. Moreover, the Ag/GO nanocomposite was also useful for the detection of Cd^{2+} ions in an aqueous solution with a detection limit of 10.15 mg/L. This study developed an eco-friendly route for the fabrication of Ag/GO nanocomposite using a non-toxic procedure that could be a great potential for biomedical-related applications and colorimetric detection of heavy metal present in water.

Introduction

Silver nanoparticles (AgNPs) have a large specific surface area and unique physical and chemical properties that have attracted much more attention to investigate in the field of antibacterial. AgNPs released Ag+, which makes bacteria demolition [1]. Nevertheless, AgNPs tend to agglomerate to decrease the surface energy, which results in reducing the antibacterial activity. Therefore, the necessity of a new material that stabilizes the AgNPs is required [2].

Graphene oxide (GO) is a widely used material in many fields due to its unique properties. The structure of the GO sheets has sharp edges and contains lots of oxygen functional groups on its surface, resulting in a large specific surface area that interacts well with the bacterial cell membranes [3]. Hence, the silver-based graphene oxide nanocomposite (Ag/GO) was synthesized to increase the AgNPs stability and evenly disperse on the GO surface, thereby enhancing the antibacterial activity. In addition, AgNPs have molar attenuation coefficients or light scattering effects highly, and surface plasmon bands can change in size and distance, along with a large interactive surface area. Furthermore, Ag^+ was released from AgNPs anchoring on the GO sheets exhibits a surface plasmon resonance absorption band, which is highly susceptible as contacted to other inorganic contaminants [4].

In this study, Ag/GO was synthesized via the *in-situ* method. The characterization was analyzed by X-ray diffraction, Transmission electron microscopy, Raman spectroscopy, energy-dispersive X-ray spectroscopy, and UV-Vis spectroscopy. The antibacterial capacity of Ag/GO was investigated on two Gram-negative bacteria strains (*Escherichia coli* ATCC 25922 (*E. coli*), Pseudomonas aeruginosa ATCC 27853 (*P. aeruginosa*)) and Gram-positive (*Staphylococcus aureus* ATCC 25923 (*S. aureus*)) by measuring the zone diameter inhibition and the prospect of detecting the pollutant heavy metal ion (Cd^{2+}) domestic is also simultaneously evaluated.

Experimental

Materials and chemicals

Graphite (particle size <20 μm) and silver nitrate ($AgNO_3$) were purchased from Sigma Aldrich Co. Ltd., USA. Potassium permanganate ($KMnO_4$), ammonium hydroxide (NH_3), ethanol (C_2H_6O), and D-glucose ($C_6H_{12}O_6$) were purchased from ChemSol, Vietnam. Sulfuric acid (H_2SO_4), phosphoric acid (H_3PO_4), and hydrogen peroxide (H_2O_2) were purchased from Xilong, China. Note that all mentioned chemicals were used without further purification. Bacteria *E. coli*, *P. aeruginosa*, and *S. aureus* were purchased from Pasteur Institute in Ho Chi Minh City, Vietnam.

Synthesis of GO

GO was synthesized by the improved Hummers' method. Briefly, 3g of graphite powder was slowly added to a mixture of 360 mL H_2SO_4 and 40 mL H_3PO_4

within stirring at less than 20 °C. Then, $KMnO_4$ (18.0 g) was slowly added to the solution, followed by heating to 50 °C under constant stirring for 12 h. After that, the mixture was cooled off and added with 500 mL distilled water via 15 mL H_2O_2, resulting in bright yellow solution. It was then centrifuged and washed with distilled water and ethanol before being dried at 60 °C for 24 h to obtained solid graphite oxide (GiO). The GiO was dispersed in water to get the concentration of 5 mg/mL in an ultrasonic bath. After 12 h of ultrasonication treatment, GO suspension was obtained.

Synthesis of Ag/GO

Ag/GO was fabricated via the *in-situ* method using glucose as a green reducing agent. Firstly, 500 mg of $AgNO_3$ was suspended in 500 mL distilled water within drop-wise adding NH_3 to reach the pH of 10. Next, 100 mL $AgNO_3/NH_3$ solution was added to 100 mL GO suspension (5 mg/mL) and then ultrasound (1080 W) at 60 °C for 60 min in the bath. After that, the mixture was blended with 50 mL glucose solution (10 mg/mL), which was continued stirring at 60 °C for 1 h. The prepared solution was cooled to room temperature, then centrifuged, and washed with distilled water and ethanol. Finally, Ag/GO in powder form was obtained after drying at 60 °C for 24 h.

Characterization

X-ray diffraction (XRD) was investigated by using Advanced X8, Bruker (λX = 0,154 nm) with CuKα irradiation in the range of 5~80°. Transmission electron microscopy (TEM) images (S-4800, Hitachi, Japan) of the materials were carried out at an accelerating voltage of 100 kV. The composition of elements (C, O, and Ag) in the composite was determined via the Energy-dispersive X-ray spectroscopy (EDS) (Jeol-JMS 6490, Japan). Raman spectra were conducted by using a LabRam micro-Raman system at an excitation wavelength of 632 nm (He-Ne laser).

Antibacterial activity

The antibacterial activity of Ag/GO against three strains of bacteria: *E. coli*, *P. aeruginosa*, and *S. aureus* was determined by using the agar plate diffusion method. The bacteria were cultivated and propagated in Lysogeny Broth for 24 h. Following that, three samples of Ag/GO with different concentrations (1.25, 0.625, and 0.3125 mg/mL) were prepared by diluting the

initial 10 µL Ag/GO solution. Subsequently, each concentration was added dropwise onto each 6 mm diameter paper plate before being placed on the bacteria-inoculated agar plate and incubated at 37 °C for 24 h. The antibacterial effect is assessed based on the antibacterial ring diameter that covers the material. Gentamicin and distilled water were used as the positive and negative controls of the test, respectively. All experiments were repeated three times.

Cd^{2+} detection

The Cd^{2+} solution was diluted comprehensively to various concentrations (0-200 mg/L) whereby 5 mL aliquots of each solution were extracted slowly into 10 mL test tubes followed by adding 40 µL of suspended Ag/GO solution (10 g/L) to each tube within shaking for 2 minutes. The mixture was analyzed with UV-Vis spectrometry maximum absorbance band of Ag/GO at 422 nm and the linear relationship between the Cd^{2+} concentration and the absorbance band of the material. The obtained linear equation is then statistical analyzed by Origin 2019b software to determine its linearly regression via the slope, intercept, and the standard deviation. The LOD and LOQ were calculated based on the standard deviation (SD) of the response and the slope, as shown in Equation (1) and (2):

$$LOD = 3.3 \times \frac{\sigma}{S} \qquad (1)$$

$$LOQ = 10 \times \frac{\sigma}{S} \qquad (2)$$

where LOD: limit of detection; LOQ: limit of quantification; σ: standard deviation of the response; S: the slope of the as-prepared line [5]. The standard error (SE) of y-intercepts of regression lines may be used as the SE of the response and it is also related to the SD and total number of samples (N) or number of observations by the Equation (3):

$$SE = \frac{\sigma}{\sqrt{N}} \qquad (3)$$

Therefore, the σ can be recognized by multiplying the SE with square root of N.

Results and discussion

Characterization of Ag/GO

As shown in Fig 1a and b, the TEM images of Ag/GO shows that AgNPs were evenly distributed on the GO surface around 15-30 nm in size. This uniform distribution shows that the GO plays an important role to reduce and inhibit the agglomeration and also stabilization the size of AgNPs [6]. According to the XRD pattern, there are diffraction characteristic peaks at 2θ = 38, 44, 65, and 78°, corresponding to (111), (200), (220), and (311) crystal planar, respectively (Fig 1c).
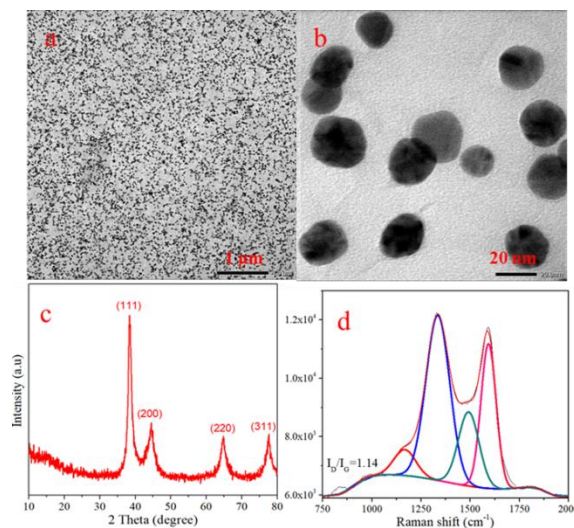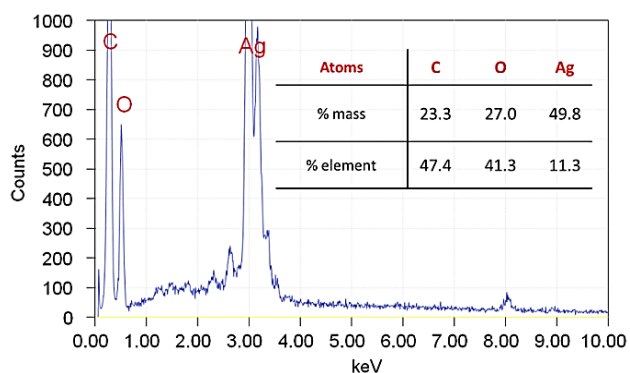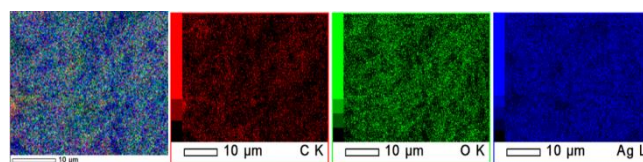

Figure 1: TEM images at (a) 1 µm and (b) 20 nm; (c) XRD pattern, and (d) Raman spectrum of Ag/GO

(a)

(b)

Figure 2: (a) EDS spectrum and (b) X-ray mapping images of Ag/GO

The diffractions match well with the standard AgNPs peaks (JCPDS file no. 04-0783) and prove the existence of the Ag molecule in the GO matrix with high

crystallinity [7]. In the Raman spectrum of Ag/GO (Fig 1d), the increasing in I_D/I_G ratio shows a lower level of C-sp^2 regions with a high disorder in the planar structure during the reducing process, therefore increasing the space for grafting the AgNPs and also improving the Raman scattering of the nanocomposite. The spectra are indicative of carbonaceous-material: disordered carbon (D1 at 1165 cm^{-1}), amorphous carbon (D3 at 1500 cm^{-1}), and ordered carbon (G at 1530 cm^{-1}) [8].

The analysis results of components of Ag/GO with element composition are shown in Fig 2a while the distribution of elements on Ag/GO is observed in Fig 2b. Numerous spherical Ag are uniformly distributed on the surface of GO sheets. These results are in good agreement with TEM images [9].

Antibacterial activity

The antibacterial investigation via inhibition zone diameter of Ag/GO for the three bacterial strains was shown in Fig 3. In which, the inhibition zone diameter for *E. coli*, *P. aeruginosa*, and *S. aureus* increased as increasing Ag/GO concentration from 0.3125 to 1.25 mg/mL. Occasionally, the higher amount of the nanomaterial revealed the enhancement in the interaction among the bacteria with AgNPs surface and GO sheets, which greatly promote the antimicrobial process [10]. The oxygenated functional groups via the delocalized conjugated π region in GO could end up forming the hydrogen bonding with the bacterial membrane while Ag$^+$ ions released from equation (3) under the adequate condition to penetrate the cell membrane of bacteria [11]:

$$4Ag+O_2+4H^+ \rightarrow 4Ag^+ +2H_2O \qquad (3)$$
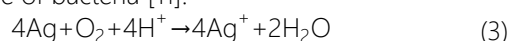
Afterward, the Ag$^+$ was claimed to alter the membrane components; inactivate its replication and respiration; damage the proteins, lipids, and DNA by various reactive oxygen species proceeding during the oxidation process, eventually cause cell death [12].

For *P.aeruginosa*, the antibacterial performance of Ag/GO was the highest with an antibacterial ring diameter of approximately 25 mm, corresponding to an Ag/GO concentration of 1.25 mg/mL. The cell wall of *P. aeruginosa* was recognized as thinner than that of *S. aureus* for accessible penetration, which facilitates for the material against bacteria easily. In specific, various efflux pumps owning in its cell could dislodge away the antimicrobial agents, thus attempting to more Ag/GO injection is further impractical. One more point, the Gram-negative bacteria likewise *E. coli* has

an outer covering of phospholipids and Lipo-polysaccharides, which impart a strong negative charge to the surface of Gram-negative bacterial cells [13]. Therefore, from 0.3125 to 0.625 mg/mL, the ring diameter decrease due to the poor interaction with the negatively charged surface of the material while at 1.25 mg/mL, the probability for the collision with the material is higher, so the performance is well improved. Regarding the comparison between the controls samples, it is noteworthy that Ag/GO materials possessed superior antibacterial performance compared to negative control samples being water. Besides, the antibacterial ring size of Ag/GO samples at the concentration of 1.25 mg/L was nearly equal to the positive control samples, which is gentamicin. In particular, for *E. coli* and *S. aureus*, Ag/GO at the concentration of 1.25 mg/L had an antibacterial diameter of 16 and 23 mm, respectively, which were approximately close to that of positive control samples of 20 mm and 25 mm. *P. aeruginosa* bacteria has the highest antibacterial ring diameter of 25 mm at an Ag/GO concentration of 1.25 mg/L, which was not considerably different from the positive control of 30 mm. Those results show the potential application of Ag/GO as a superior antibacterial material.
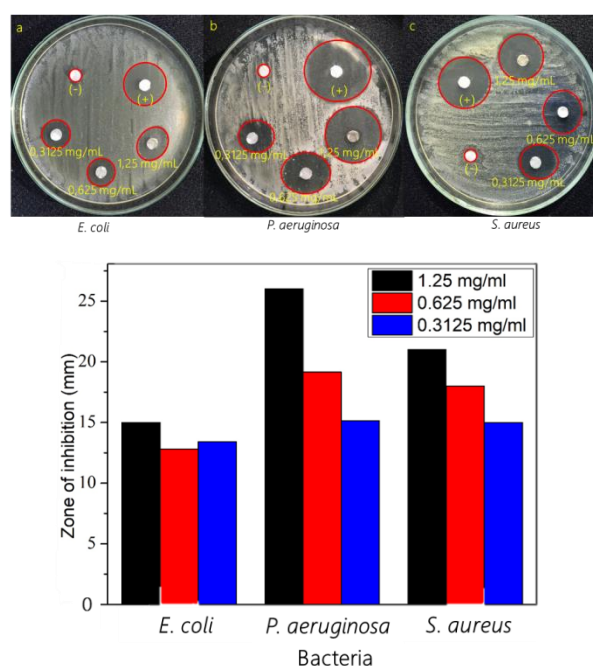

Figure 3: The zone inhibition of (a) *E. coli*, (b) *P. aeruginosa*, (c) *S. aureus*, and (d) zone inhibition chart

Cd^{2+} detection

Figure 4 illustrated the UV-Visible spectra of Ag/GO in the presence of Cd^{2+} in the range of 0-200 mg/L. The

surface plasmon resonance (SPR) absorption band in AgNPs has employed a vital role in sensing the inorganic contaminants traces [14]. Particularly, the SPR band at 420 nm nearly witnessed a remarkable decrease upon the Cd^{2+} concentration is controlled higher amount. Once the injection to the medium within the silver detector, the metallic cation will be adsorbed onto the material by the electrostatic force drawn by the oxygen-containing group via high C-sp^2 regimes in the GO matrix. At this point, due to the lower redox potential of Cd^{2+}/Cd than Ag^+/Ag (-0.400 as compared with 0.7996 V), the oxidation of AgNPs anchoring on GO nearby to Ag^+ could not occur, but the aggregation of AgNPs caused by the structural binding between the cation and the GO basal plane is predominant, affirming the change in color and also the SPR band of the AgNPs [15].

The reduction of the mono-dispersity of the Ag molecule in GO and removal of GO from those particles of the Cd traces has well accompanied with the downward band shift from 420 to 330 nm. The higher charge transportation due to the potent conjugated π-π areas in GO inducing for various series binding GO-Cd-GO matrix has subsequently participated in the efficiency of the sensing process in a shorter time [16].
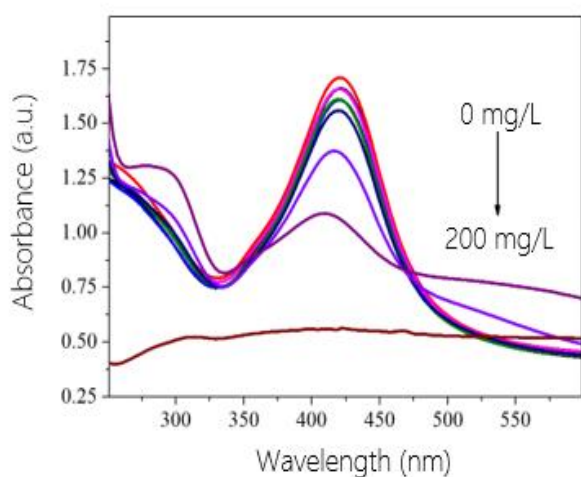
Figure 4: UV-Vis absorbance of Ag/GO with different Cd^{2+} concentration

The results were linearly sketched as shown in Fig 5. It exhibited an acceptable linear relationship between the value of absorbance and the Cd^{2+} concentration over the range of 0-200 mg/L with a linear regression coefficient (R^2) of 0.9985, LOD of approximately 10.15 mg/L and LOQ of 30.75 mg/L. These values were relatively low compared to some other researches as shown in Table 1.

The table implied the presence of the carbonaceous material, especially GO in maintaining the stability of the Ag molecules and sorption up-taking toward metallic cation, aid in the improvement of the sensing performance. The uniform grafting on the GO sheets of AgNPs could prevent the stagnant of GO, thus make more space for binding with Cd^{2+}. The hydroxyl and carbonyl groups of GO with higher charge density were claimed to accompany an effective linking with the trace cation and afterward, form the stable complexes with them. All things considered, the modification of GO with Ag has enhanced the response of Cd^{2+} detection.
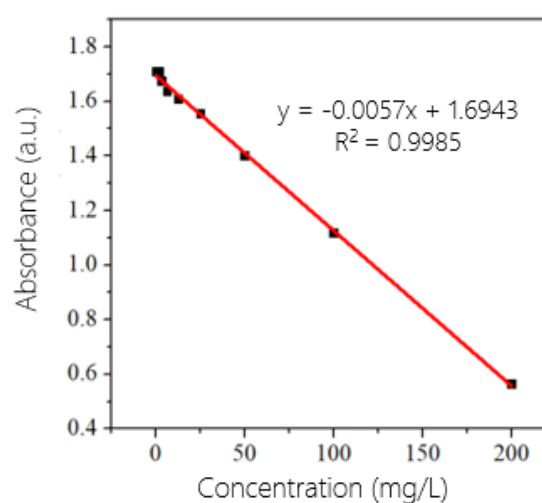
Figure 5: The linear relationship between absorbance at 420 nm and Cd^{2+} concentration

Table 1: Comparison of the LOD of Cd^{2+} with other researches

No.	Material	LOD (mg/L)	Reference
1	AgNPs	0.198	[17]
2	AgNPs	0.06	[18]
3	AgNPs	0.034	[19]
4	Ag/Graphene	0.017	[20]
5	Ag/GO	10.15	This work

Conclusion

Ag/GO nanocomposite was successfully fabricated via in-situ method, eco-friendly and non-toxic procedure. The AgNPs were uniformly distributed on the surface of GO with an average size of 15-30 nm. The antibacterial tests on *E. coli*, *P. aeruginosa*, and *S. aureus*, indicated that Ag/GO exhibited the highest

performance on *P. aeruginosa* with the zone diameter inhibition of about 25 mm and the Ag/GO concentration of 1.25 mg/mL. Additionally, the synthesized Ag/GO displayed the prospect of heavy metal detection with the LOD of 10.15 mg/L for Cd^{2+}. The obtained results indicated that Ag/GO could be used as potential antibacterial material for biomedical application and colorimetric detection of heavy metal in water.

Acknowledgments

References

1. D. Gu, X. Chang, X. Zhai, S. Sun, Z. Li, T. Liu, L. Dong, and Y. Yin, Int. 42 (2016) 9769–9778. https://doi.org/10.1016/j.ceramint.2016.03.069
2. D. Vilela, M. C. González, and A. Escarpa, Anal. Chim. Acta 751 (2012) 24–43. https://doi.org/10.1016/j.aca.2012.08.043
3. S. Liu, T. Helen Zeng, M. Hofmann, E. Burcombe, J. Wei, R. Jiang, J. Kong, and Y. Chen, ACS Nano 5 (2011) 6971–6980. https://doi.org/10.1021/nn202451x
4. S. K. Kailasa, J. R. Koduru, M. L. Desai, T. J. Park, R. K. Singhal, and H. Basu, TrAC Trends Anal. Chem. 105 (2018) 106–120. https://doi.org/10.1016/j.trac.2018.05.004
5. A. Virgilio, A. B. S. Silva, A. R. A. Nogueira, J. A. Nóbrega, and G. L. Donati, J. Anal. At. Spectrom. 35 (2020) 1614–1620. https://doi.org/10.1039/D0JA00212G
6. S. S. I. Abdalla, H. Katas, J. Y. Chan, P. Ganasan, F. Azmi, and M. F. M. Busra, RSC Adv. 10 (2020) 4969–4983. https://doi.org/10.1039/C9RA08680C
7. N. Minh Dat, V. N. P. Linh, N. T. L. Phuong, L. N. Quan, N. T. Huong, L. A. Huy, H. M. Nam, M. Thanh Phong, and N. H. Hieu, Technol. 34 (2019) 792–799. https://doi.org/10.1080/10667857.2019.1630898
8. C. Castiglioni and M. M. S. Tommasini, (2007).
9. N. X. Dinh, N. Van Cuong, N. Van Quy, T. Q. Huy, K. Mølhave, and A.-T. Le, J. Electron. Mater. 45 (2016) 5321–5333. https://doi.org/10.1007/s11664-016-4734-8
10. L. C. Yun'an Qing, R. Li, G. Liu, Y. Zhang, X. Tang, J. Wang, H. Liu, and Y. Qin, Int. J. Nanomedicine 13 (2018) 3311. https://doi.org/10.2147/IJN.S165125
11. N. Minh Dat, V. N. P. Linh, L. A. Huy, N. T. Huong, T. H. Tu, N. T. L. Phuong, H. M. Nam, M. Thanh Phong, and N. H. Hieu, Mater. Technol. 34 (2019) 369–375. https://doi.org/10.1080/10667857.2019.1575555
12. V. Palmieri and M. Papi, Nano Today 33 (2020) 100883. https://doi.org/10.1016/j.nantod.2020.100883
13. N. Malanovic and K. Lohner, Biophys. Acta (BBA)-Biomembranes 1858 (2016) 936–946. https://doi.org/10.1016/j.bbamem.2015.11.004
14. N. M. Dat, T. H. Quan, D. M. Nguyet, T. N. M. Anh, D. B. Thinh, T. C. Diep, L. A. Huy, L. T. Tai, N. D. Hai, P. T. Khang, H. M. Nam, M. T. Phong, and N. H. Hieu, Appl. Surf. Sci. 551 (2021) 149434. https://doi.org/10.1016/j.apsusc.2021.149434
15. K. Arora, Nanomaterials Handb. Graphene, Vol. 6 Biosens. Adv. Sensors (2019) 297.
16. N. Karki, H. Tiwari, C. Tewari, A. Rana, N. Pandey, S. Basak, and N. G. Sahoo, J. Mater. Chem. B 8 (2020) 8116–8148. https://doi.org/10.1039/D0TB01149E
17. J. Du, X. Hu, G. Zhang, X. Wu, and D. Gong, Anal. Lett. 51 (2018) 2906–2919. https://doi.org/10.1080/00032719.2018.1455103
18. F. Tanvir, A. Yaqub, S. Tanvir, R. An, and W. A. Anderson, Materials (Basel). 12 (2019) 1533. https://doi.org/10.3390/ma12091533.
19. M. L. Firdaus, I. Fitriani, S. Wyantuti, Y. W. Hartati, R. Khaydarov, J. A. Mcalister, H. Obata, and T. Gamo, Anal. Sci. 33 (2017) 831–837. https://doi.org/10.2116/analsci.33.831
20. S. Palisoc, E. Lee, M. Natividad, and L. Racines, Int. J. Electrochem. Sci. 13 (2018) 8854. https://doi.org/10.20964/2018.09.03